HHS Public Access

Author manuscript

Nature. Author manuscript; available in PMC 2014 December 19.

Published in final edited form as:

Nature. 2014 June 19; 510(7505): 412–416. doi:10.1038/nature13261.

CFIm25 links Alternative Polyadenylation to Glioblastoma Tumor Suppression

Chioniso P. Masamha[1,*], **Zheng Xia**[2,*], **Jingxuan Yang**[3], **Todd R. Albrecht**[1], **Min Li**[3], **Ann-Bin Shyu**[1,#], **Wei Li**[2,#], and **Eric J. Wagner**[1,#]

[1]Department of Biochemistry and Molecular Biology, The University of Texas Medical School at Houston. Houston, TX

[2]Division of Biostatistics, Dan L Duncan Cancer Center and Department of Molecular and Cellular Biology, Baylor College of Medicine, Houston, TX

[3]The Vivian L. Smith Department of Neurosurgery, The University of Texas Medical School at Houston. Houston, TX

Abstract

The global shortening of mRNAs through alternative polyadenylation (APA) that occurs during enhanced cellular proliferation represents an important, yet poorly understood mechanism of regulated gene expression[1,2]. The 3′UTR truncation of growth promoting mRNA transcripts that relieves intrinsic microRNA- and AU-rich element-mediated repression has been observed to correlate with cellular transformation[3]; however, the importance to tumorigenicity of RNA 3′ end processing factors that potentially govern APA is unknown. Here, we have identified CFIm25 as a broad repressor of proximal poly(A) site usage that, when depleted, increases cell proliferation. Applying a regression model on standard RNA-seq data for novel APA events, we identified at least 1,450 genes with shortened 3′UTRs after CFIm25 knockdown, representing 11% of significantly expressed mRNA in HeLa cells. Dramatic increases in expression of several known oncogenes including Cyclin D1 are observed as a consequence of CFIm25 depletion. Importantly, we identified a subset of CFIm25-regulated APA genes with shortened 3′UTRs in glioblastoma (GBM) tumors that have reduced CFIm25 expression. Downregulation of CFIm25 expression in glioblastoma cells enhances their tumorigenic properties and increases tumor size while CFIm25 overexpression reduces these properties and inhibits tumor growth. These findings identify a

[#]To whom correspondence should be addressed: Eric J. Wagner, Department of Biochemistry and Molecular Biology, University of Texas Medical School, (Eric.J.Wagner@uth.tmc.edu); Ann-Bin Shyu, Department of Biochemistry and Molecular Biology, University of Texas Medical School, (Ann-Bin.Shyu@uth.tmc.edu); Wei Li, Dan L Duncan Cancer Center and Department of Molecular and Cellular Biology, Baylor College of Medicine, (WL1@bcm.edu).

[*]contributed equally to this manuscript

Author Contributions. A-B.S., W.L., and E.J.W. designed the study. C.P.M., T.A., and J.X. performed the described experiments with conceptual advice from M.L.. W.L. and Z.X. conducted bioinformatic analyses and developed the DaPars algorithm. C.P.M., Z.X., W.L., A-B.S. and E.J.W. wrote the manuscript.

The authors declare no competing interests as defined by Nature Publishing Group, or other interests that might be perceived to influence the results and discussion reported in this paper.

Raw sequence data is available in the Gene Expression Omnibus (GEO) database under accession number GSE42420.

pivotal role of the CFIm25 in governing APA and reveal a previously unknown connection between CFIm25 and glioblastoma tumorigenicity.

Recently, it has become increasingly clear that mRNA 3′ end formation is subject to dynamic regulation under diverse physiological conditions[2-5]. Over 50% of human genes have multiple polyadenylation signals, thereby increasing the potential diversity in mRNA transcript length[6]. The formation of mRNA transcripts using these distinct poly(A) sites (PASs) is carried out by APA with the most common form involving differential use of alternative PASs located within the same terminal exon (reviewed in [7]). Processing at a PAS most proximal to the stop codon (pPAS) removes negative regulatory elements that reduce mRNA stability or impair translation efficiency such as AU-rich elements (AREs)[8] and microRNA (miRNA) targeting sites[9,10]. It has been reported that both rapidly proliferating cells[1,2] and transformed cells[3,11] preferentially express mRNAs with shortened 3′UTRs. Despite these observations, the mechanisms that control the extensive distal to proximal PAS switch observed in proliferative and/or transformed cells, the cause-and-effect relationship, as well as the critical target genes subject to this regulation, are not well-characterized.

To measure relative changes in endogenous APA events, we devised a quantitative RT-PCR (qRT-PCR) assay to monitor the transcript-specific use of the distal PAS (dPAS) while normalizing for total mRNA levels for three test transcripts, Cyclin D1, Dicer1, and Timp2 known to undergo APA[3,12]. Using this approach, we readily detected appreciable usage of dPASs for all three genes in HeLa cells (Extended Data Fig. 1). This was somewhat surprising given their highly transformed state, but is consistent with previous reports that not all transformed cells tested exhibit appreciable 3′UTR shortening[1,3]. Previous studies implicate multiple members of the cleavage and polyadenylation (CPA) machinery as potentially regulating poly(A) site selection[12-15]. To test the relative contribution of these factors to the APA of the three test genes, we utilized systematic RNAi (Fig. 1a-c). We observed only small changes in the relative use of the dPAS after knockdown of members of the CPSF/CstF/CFIIm complexes (Fig. 1d-e). In contrast, we detected significant reduction in dPAS usage after knockdown of the members of the CFIm complex. These results are consistent with a recent report that CFIm68 depletion decreases 3′UTR length[14]; however, the most significant PAS switching was found to occur after knockdown of CFIm25. We therefore focused all further analyses on CFIm25.

Traditional methods of global PAS profiling utilize mRNA partitioning and digestion to sequence poly(A) junctions within messages[1,16,17]. To identify global targets of CFIm25 with a more streamlined approach requiring less sample manipulation, we performed high-depth (>3.0×10^8 reads) RNA sequencing (RNA-seq) after knocking down CFIm25 in parallel with a control knockdown. We determined that 23% of RNA-seq reads can be uniquely mapped to 3′UTRs of expressed genes leading to approximately 200-fold sequence coverage (Extended Data Fig. 2a/b). We first analyzed the three test genes and observed dramatically reduced read density within the 3′UTRs in response to CFIm25 depletion (Fig. 2a). These results not only confirm our qRT-PCR findings that HeLa cells robustly utilize the dPAS for all three test genes under basal conditions but also demonstrate that significant

3′UTR shortening induced by CFIm25 knockdown is readily visualized by analyzing the read density of RNA-seq data.

Based on this promising observation, we applied a novel bioinformatics algorithm termed "Dynamic Analysis of Alternative Polyadenylation from RNA-Seq" (DaPars; see Supplemental Methods) for the *de novo* identification of all instances of 3′UTR alterations between control and CFIm25 knockdown cells, regardless of a pre-annotated pPAS within each Refseq transcript. DaPars uses a linear regression model to identify the exact location of this novel proximal 3′UTR as the optimal fitting point (red point in Fig. 2b) as well as the abundance of both novel and annotated UTRs. The degree of difference of 3′UTR usage between the samples was then quantified as a change in percentage dPAS usage index (ΔPDUI), which is capable of identifying lengthening (positive index) or shortening (negative index) within the 3′UTR. When applied to the 12,273 RefSeq transcripts whose average terminal exon sequence coverage is more than 30-fold, DaPars identified 1,453 transcripts possessing a significant, reproducible shift in 3′UTR usage in response to CFIm25 depletion (Fig. 2c and Extended Data Fig. 2c/d). Strikingly, among this group of transcripts, 1,450 are shifted to proximal PAS usage in CFIm25 knockdown. We found a significant enrichment of the CFIm25 UGUA binding motif and previously reported CFIm25 iCLIP sequence tags[14] within 3′UTRs that shortened after CFIm25 knockdown relative to transcripts exhibiting no length change (Extended Data Fig. 3). Moreover, we determined that 70% of transcripts whose 3′UTR is shortened after CFIm25 knockdown, utilize a pPAS within the first one-third of their 3′UTR. In contrast, only 29% of multi-PAS transcripts that did not alter 3′UTR length in response to CFIm25 have an annotated pPAS in the first one-third of their 3′UTR. This demonstrates that CFIm25 APA targets are enriched with pPASs positioned close to the stop codon to maximize their degree of 3′UTR shortening. Collectively, these results clearly indicate that the function of CFIm25 is to broadly repress proximal poly(A) site choice, and consequently, the shortening of 3′UTR length is dramatic for the majority of CFIm25 regulated transcripts upon its depletion.

One potential consequence of 3′UTR shortening in CFIm25 knockdown is the loss of miRNA binding sites and/or AREs resulting in truncated mRNA transcripts that evade negative regulation. Although the correlation between transcript expression change and ΔPDUI was modest (Pearson correlation= -0.25), it does reveal that transcripts with shorter 3′UTR in CFIm25KD have overall higher expression levels (Fig. 2d). We observed that 64% of transcripts with shortened 3′UTRs exhibited significantly increased steady-state levels, 34% were unchanged, and only 2% were significantly reduced (Extended Data Fig. 4). We have also organized the list of CFIm25-regulated genes with respect to their ΔPDUI score, change in relative levels of transcript, and predicted numbers of AREs and microRNA target sites lost after APA (Table S1) and observed that gene expression positively correlates with the number of lost AREs and miRNA target sites (Extended Data Fig. 5). Several examples of novel genes whose APA is regulated by CFIm25 is shown in Figure 2e and it is important to note that not all long 3′UTRs were observed to shorten in response to CFIm25 knockdown, indicating that the CFIm complex regulates many, but not all genes capable of APA (Fig. 2f). Collectively, these data demonstrate the power and ease of the DaPars

algorithm to identify APA within standard RNA-seq and indicate that the major form of CFIm25 regulation is to repress proximal PAS choice at a global level.

In order to validate the ΔPDUI results, we created qRT-PCR amplicons to monitor dPAS usage of six genes whose 3′UTRs were found to be shortened after CFIm25 knockdown and two observed not to be altered. Using these amplicons, we analyzed RNA isolated from cells effectively depleted of CFIm25 using two independent siRNAs (Fig. 3a, figure inset), and observed high congruence between qRT-PCR results and with those obtained using RNA-seq/ΔPDUI (Fig. 3a, graph). To formally test for the presence of de-repressed protein expression from mRNAs with shortened 3′UTRs, we measured their levels in lysates from knockdown cells (Fig. 3b). We observed significant increases in protein levels of CFIm25 target genes including several that have a well-documented importance to tumor growth including Cyclin D1, Glutaminase, and methyl-CpG-binding protein 2 (MecP2)[18-22]. It is worth noting that the 3′UTR of each of these genes has been shown to be subject to microRNA-mediated inhibition[23-25]. Consistent with this observation, we also noted enhanced cellular proliferation in response to knockdown of CFIm25 relative to control knockdown in HeLa cells (Fig. 3c). Finally, to determine if the 3′UTR is sufficient to elicit translational de-repression to a heterologous protein in response to CFIm25 knockdown, we used reporters with the Smoc1 3′UTR cloned downstream of luciferase or the GAPDH 3′UTR, which was not found to alter its poly(A) site usage. We observed that only the luciferase activity specifically resulting from Luc-Smoc1 message was increased in response to knockdown of CFIm25 (Fig. 3d) supporting the notion that the increased expression in endogenous Smoc1 protein, when CFIm25 is depleted, is mediated through its 3′UTR.

The collective observations that CFIm25 depletion leads to broad 3′UTR shortening, enhanced expression of growth promoting genes, and increased cell proliferation support the hypothesis that CFIm25 is a novel anti-proliferative gene whose levels may be reduced in human cancers. We focused our analysis on glioblastoma (GBM) as recent reports indicate that brain tissue possesses the longest 3′UTRs[26,27]. We reasoned that tumors derived from these cells might be more sensitive to changes in CFIm25 levels than other cancers. To test this prediction, we downloaded archived patient RNA-seq data from TCGA, stratified it according to CFIm25 expression, and analyzed it using DaPars. Indeed, following the same cutoffs in our HeLa RNA-seq 3′UTR analysis, we identified 60 genes with altered 3′UTRs and 59 of those experienced shortening in GBM (Fig. 4a and Table S2). Among those genes, a significant number of events (24 genes; P=2.2e-12 by hypergeometric testing) also shortened in CFIm25 knockdown HeLa cell line and this percentage of overlap increased dramatically to 86% as the ΔPDUI cutoff increased from 0.2 to 0.4 (Extended Data Fig. 6). Two representative examples of genes, Fos-related antigen 2 (Fra-2) and MecP2, with shortened 3′UTRs in low CFIm25 expressing GBM tumors is shown in Figure 4b demonstrating a compelling similarity between the patient samples and HeLa cells before and after CFIm25 knockdown. Overexpression of either of these genes has been shown to enhance cell proliferation[18,28].

To formally test if altering CFIm25 expression can modulate GBM tumorigenic properties, we screened a panel of GBM cell lines and observed that U251 cells naturally express lower levels of CFIm25 compared to LN229 cells, which express higher levels (Fig. 4c). To raise

CFIm25 levels in U251 cells, we created cell lines stably expressing either myc-tagged CFIm25 or GFP as a control. In parallel, we used RNAi to reduce CFIm25 levels in LN229 cells (Fig. 4c). We observed a significant reduction in anchorage-dependent growth and cellular invasion in U251 cells overexpressing CFIm25 compared to the GFP control whereas reducing CFIm25 in LN229 cells caused an increase in both of these properties (Extended Data Fig. 7). To determine if the altered *in vitro* properties of GBM cells affected tumor growth kinetics *in vivo*, we utilized a subcutaneous xenograft model. Increased expression of CFIm25 in U251 resulted in a dramatic reduction in tumor growth and decreased tumor cell proliferation (Fig. 4d and Extended Data Fig. 8). In contrast, depletion of CFIm25 in LN229 cells caused a profound increase in tumor size (Fig. 4f and Extended Data Fig. 9). Collectively, these results uncover a tumor suppressive property of CFIm25 in GBM that is likely mediated through its broad repression of APA-dependent mRNA 3′UTR shortening.

In this study, we identified CFIm25 among 15 cleavage and polyadenylation factors as a key factor that broadly regulates APA. Importantly, the data presented here also extends our understanding of APA in regulated gene expression through the demonstration that extensive shortening of 3′UTRs causally leads to enhanced cellular proliferation and tumorigenicity, likely through the upregulation of growth promoting factors, such as Cyclin D1. These results vividly describe the importance of 3′UTR usage in cell growth control and underscore the need for further research into the mechanism and regulation of APA and its potential links to other human diseases.

Methods

RNA-seq

We employed whole transcriptome RNA-seq to investigate alternative PAS usage in a genome-wide fashion. Two control and two CFIm25 knockdown samples were sequenced by HiSeq 2000 (LC Sciences). 101×2 paired-end RNA-seq reads were aligned to the human genome (hg19) using TopHat 2.0.10[30]. RefSeq gene expressions were quantified by RSEM[31]. The statistical summary of reads alignment and average gene expressions were in Extended Data Figure 2. More than 12,000 (∼50%) human RefSeq genes can be detected through RNA-seq with expression levels more than 1 FPKM (fragments per kilobase of transcript sequence per million mapped paired-end reads)[32]. More importantly, average of 23% of RNA-seq reads can be uniquely mapped to 3′UTRs of expressed genes that renders around 200x coverage on UTRs. Raw sequence data is available in the Gene Expression Omnibus (GEO) database under accession number GSE42420. All the TCGA GBM RNA-seq BAM files were downloaded from the UCSC Cancer Genomics Hub (CGHub, https://cghub.ucsc.edu/).

Analysis of Alternative Polyadenylation from RNA-seq

We used a novel bioinformatics algorithm DaPars (unpublished data; https://code.google.com/p/dapars) for the *de novo* identification of Alternative Polyadenylation from RNA-seq. The observed sequence coverage was represented as a linear combination of novel and annotated 3′UTRs. For each RefSeq transcript with annotated PAS, we used a

regression model to infer the end point of alternative novel PAS within this 3′UTR at single nucleotide resolution, by minimizing the deviation between the observed read coverage and the expected read coverage based on two-PAS model, in both control and CFIm25KD samples simultaneously.

In order to quantify the relative PAS usage, we defined the percentage of distal PAS usage for each sample as PDUI index. The greater the PDUI is, the more distal PAS of a transcript is used and vice versa.

Differential Percentage of Distal PAS Usage Index (ΔPDUI)

We used the following three criteria to detect the most significant shifted 3′UTR events: First, given the expression levels of short and long 3′UTR in two samples in each condition, we compute the significance of the difference of mean PDUIs using Fisher's exact test, which is further adjusted by Benjamini-Hochberg (BH) procedure to control false discovery rate (FDR) at 5% level. Second, the absolute difference of mean PDUIs must be no less than 0.2. Third, the absolute log2-ratio (fold-change) of mean PDUIs must be no less than 1. To avoid false positive estimation on low coverage transcripts, we required that there is more than 30 fold coverage on the 3′UTR region of both samples. For genes with multiple annotated PASs, we only kept the one with greatest |ΔPDUI| value. Finally, we identified 1,453 transcripts possessing significant shift in 3′UTR usage in response to CFIm25 knockdown, the vast majority of which have shortened 3′UTR in CFIm25 knockdown.

Bioinformatic analyses of 3′UTR shortening

Since miRNA binding sites and other regulatory sequences such as AU-rich element (ARE) reside in 3′UTRs[33,34], alternative polyadenylation plays an important role in mRNA stability, translation and translocation. Indeed, it has been reported that shorter 3′ UTRs produce higher levels of protein[3]. To elucidate the consequences of 3′UTR shortening, we provided the numbers of lost ARE motifs and miRNA binding sites due to the 3′UTR shortening for the transcripts shifting to proximal 3′UTR usage in CFIm25KD (Table S1). ARE is one of the most prominent cis-acting regulatory elements found in 3′ UTRs to target mRNAs for rapid degradation[35]. The eight different consensus ARE motifs including the plain AUUUA pentamer were retrieved from the ARE site database[35]. The miRNA-mRNA binding information was based on miRNA target prediction database TargetScanHuman version 6.2[36-38]. To limit the miRNA to high-confidence sites, we required probability of preferentially conserved targeting *Pct* score more than 0 for all highly conserved miRNA families[38].

Differentially expressed gene expression analysis

With two replicates in each group, we used edgeR[39] to call differentially expressed genes with FDR < 0.05. To better quantify gene expression with shorter 3′UTR, we counted reads based on the coding regions of each transcript.

Cell Culture and cell counts

All the cell lines used (HeLa, U251 and LN229) were cultured in DMEM supplemented with 10% FBS (+1% penicillin and streptomycin) in a 5% CO_2 incubator at 37°C. Cell counts were done using a standard hemacytometer.

siRNA and Western blot assays

Both siRNA transfection and Western blot analysis were performed as previously described [29]. The siRNA was purchased from Sigma and all the siRNAs used are shown below. After transfection, cells were harvested for mRNA extraction, Western Blotting or Matrigel assay. To detect 3′end processing factors by Western blotting, the following primary antibodies from Bethyl Laboratories were used: CPSF160, CPSF100, CPSF73, CPSF30, hFip, CstF77, CstF64τ, CstF50, CFIm68 and CFIm59. Other antibodies used include CFIm25 (PTGlabs), CstF64, CFIImPcf11, and Symplekin (Sigma), CFIImClp1 (Epitomics). Additional antibodies include Vma21, GLS, Acer3, and GSK3β (PTGlabs); Cyclin D1 (Cell Signaling); and SMOC1, tubulin (Abcam).

siRNA sequences used in the study

CPSF160 (si1-5′GCUUUAAGAAGGUCCCUCA, si2-5′CUUACCACGUGGAGUCUAA); CPSF100 (si1-5′CUCAACUUCUUGAUCAGAU, si2-5′GGAUAGAUGGUGUCUUAGA); CPSF73 (si1- 5′CCAUAUACUGGUCCCUUUA, si2-5′GAUAUUGGAAGUUCAGUCA); CPSF30 (si1-5′GUGCCUAUAUCUGUGAUUU, si2-5′CCUAUAUCUGUGAUUUGAA); hFip (si1-5′CGAAUGGGACUUGAAGUUA, si2-5′GACAAGUACUGCCUCCAGA); CstF77 (si1-5′GAAGACUUAUGAACGCCUU, si2-5′CACAGAAUCAACCUAUAGA); CstF64 (si1-5′GGCUUUAGUCCCGGGCAGA, si2-5′GGUUAUGGCUUCUGUGAAU); CstF64t (si1-5′GUCUUAGAGACACGUGUAA, si2-5′CUAAUGUUCUGCUGAACCA); CstF50 (si1-5′GUCGUAAGUCCGUGCACCA, si2-5′CUACUCUUCGCCUUUAUGA); Symplekin (si1-5′CAGUUCAACUCGGGCCUGA, si2-5′GAGACAUUGAGUUGCUGCU); CFIm25 (si1-5′CCUCUUACCAAUUAUACUU, si2-5′GCUAUAUACAGUGUAGAAU); CFIm59 (si1-5′CUCAUCUGCUCGUGUGGAU, si2-5′GCAAUUUCCAGCAGUGCCA); CFIm68 (si1-5′CUGCAAUUUCUUUAAUUAA, si2-5′GGAUCAAGACGUGAACGAU); CFIImClp1 (si1-5′GCUUAUGUCUCCAAGGACA, si2-5′CAGUUCAGUUGGAGUUGUU); CFIImPcf11 (si15′GUACCUUAUGGAUUCUAUU, si2-5′GUAUCUCACUGCCUUUACU) and the control siRNA used was described elsewhere[29].

qRT-PCR

After appropriate transfections, total RNA was extracted using TRIzol Reagent (Life Technologies) using the manufacturers protocol. For quantitative Real Time-PCR (qRT-PCR) the mRNA was reverse transcribed using MMLV-RT (Invitrogen) using the manufacturer's protocol to generate cDNA. The qRT-PCR reactions were performed using Stratagene MxPro3000P (Agilent Technologies) and SYBRGREEN (Fermentas). Common primers were designed to target the open reading frame and normalize for total transcript. The distal primers were designed to target sequences just before the dPAS and detect long

transcripts that use the dPAS. All primers used are shown below. Data was calculated using a modified version of the $2^{-\Delta\Delta CT}$ method to show changes in dPAS usage, where CT is the threshold cycle. First, the CT values for the common and distal was normalized to the levels of 7SK, where ΔCT (common or distal) =CT $^{\text{common or distal}}$ – CT^{7SK}. Then $\Delta\Delta CT=\Delta CT^{distal} - \Delta CT^{common}$ (note that we applied the correction factor for difference in amplification efficiency calculated in Extended Data Figure 1). To show fold changes normalized to the control siRNA transfected samples the following equation was used: normalized $\Delta\Delta\Delta CT = \Delta\Delta CT^{\text{average target siRNA}} - \Delta\Delta CT^{\text{average of control siRNA}}$. Then the decrease (-) or increase (+) in dPAS usage was calculated as +/- $2^{\text{normalized } \Delta\Delta\Delta CT}$.

Oligonucleotides used for qRT-PCR

Cyclin D1 common (F 5′- CTGCCAGGAGCAGATCGAAG, R 5′- AATGCTCCGGAGAGGAGGGACT) and distal (F 5′- ATCGAGAGGCCAAAGGCT, R 5′- CGTCTTTTTGTCTTCTGCTGGA); Dicer1 common (F 5′- CTCATTATGACTTGCTATGTCGCCTTG, R 5′- CACAATCTCACATGGCTGAGAAG) and distal (F 5′- TGCTTTCCGCAGTCCTAACTATG, R 5′- AATGCCACAGACAAAAATGACC); Timp2 common (F 5′- CAACCCTATCAAGAGGATCCAGTAT, R 5′- GATGTCGAGAAACTCCTGCTTG) and distal (F 5′- GACATCAGCTGTAATCATTCCTGTG, R 5′- CGATGCCAAATGGAGAGC); FHL1 common (F 5′- CTGGCACAAAGACTGCTTCACCTGT, R 5′- GATTGTCCTTCATAGGCCACCACACTGG) and distal (F 5′- GCCAGGGCTGTCATCAACATGGATA, R 5′- TGCATTTCAGGTAAGCGGTAGGTGGA); Tubulin common (F 5′- GAAGGCCTCATCCTCCACTTTGGAAAG, R 5′- TGCTAGCAGTGTCTCATGCTCG) and distal (F 5′- GCATCAGTAGCTGAGTGCACTCCTGGT, R 5′- GTAGAGGGTATGAAGGGCAAGAACTCT); Vma21 common (F 5′- GATAAGGCGGCGCTGAACGCACTGC, R 5′- TGAGCCTTCATTCCAGGCCACATACACA) and distal (F 5′- CATCTGCACAGCACCTTACAGTTTGC, R 5′- GAAATGCAGCACATCCAAATCCTCCC); GSK3β common (F 5′- CTGGTCCGAGGAGAACCCAATGTTTCG, R 5′- CAGCCAACACACAGCCAGCAGACCATAC) and distal (F 5′- GAGCTGAGCCCATGGTTGTGTGTAAC, R 5′- GGTTCACTTCAGCAGGCAGGACAACTC); Smoc1 common (F 5′- CTCTGATGGCAGGTCCTACGAGTCCA, R 5′- GTATGGCACTGCACCTGGGTAAAGGAG) and distal (F 5′- GAGTCCTGCAATTGTACTGCGGACTCCA, R 5′- CATGGGATCTGGACTCCCTTCCTCTC); Acer3 common (F 5′- CACGCTGGACTGGTGCGAGGAGAACT, R 5′- GTGGAAGCACCAGGATCCCATTCCTACC) and distal (F 5′- CTGTTCAAGCTAATACAGCATTTCCT, R 5′- GTGAATAAGCAGACTGAGATTACCTG); TMEM48 common (F 5′- CATTCATCCTCAGCAACTCATGCACTC, R 5′- CTGTTAGTACCAGTGCAGGGAACCAC) and distal (F 5′-

GTGCTGTGTACTAAATACAGGCCACATAGTG, R 5′-CCTGGTTCCAACAGATGGTGTGTAGA); MSRB3 common (F 5′-CTCTGGGAAGTGCGCAGTCCGGGT, R 5′- GTCCCTTTCTCCTGAGTGACATGG) and distal (F 5′- GCAGGATATGGAGTGCAATGAACTGAG, R 5′-ACAGTAAGAGCTGGAGTGCAGAGA); 7SK (F 5′GACATCTGTCACCCCATTGATC, R 5′TCTGCAGTCTTGGAAGCTTGAC)

Luciferase Assays

One day after second hit with siRNA (as above), HeLa cells were transfected with 0.25 μg of gene specific 3′UTR Rluc plasmids (Smoc-1 and GAPDH from Switchgear Genomics) using Lipofectamine 2000 (Invitrogen). Renilla luciferase activity was assayed 24 hours post-plasmid transfection using Stop and Glo reagent (Promega).

Generation of stable cell lines

LN229 cells were transfected with CFIm25 specific shRNA or control shRNA using polybrene in 6-well plates. Two days after lentiviral transfection cells were transfected with a second hit of lentivirus. Selection was done using 1ug/ml of puromycin over 2 weeks. U251 cells were transfected with either GFP or CFIm25 expressing pcDNA3 plasmids using Lipofectamine 2000 (Invitrogen) according to the manufacturer's protocol. Selection was performed over 1-2 weeks using 2.5 mg/ml of G418.

Soft agar Assay

Soft agar assays were used to determine anchorage –dependent growth. For the base layer, 1% of UltraPure low melting point agarose (Invitrogen) was mixed 1:1 with 2XDMEM media and plated in 6 well plates giving a 1.5ml bottom layer of 0.5% agar. Then 3×10^4 cells of LN229 shRNA stably transfected cells were titrated into 2XDMEM and mixed with an equal volume of 0.6% agar to give a 0.3% layer and 1.5ml was dispensed into each well. The agar was covered with 1ml of 1XDMEM and incubated in a humidified incubator at 37°C (5% CO2). Fresh media was added once a week. After 2 weeks, colonies formed were stained with 0.01% crystal violet, photographed and counted. For U251 plasmid transfected cells the same protocol was followed except that a third (0.3%) layer of agar was plated on top of the layer containing the cell suspension.

Matrigel invasion assay

The Matrigel invasion assay was performed following the manufacturer's protocol. Briefly, the 6-well BioCoat Matrigel Invasion Chamber (Becton Dickinson) was rehydrated with FBS free DMEM. The Matrigel-transwell inserts were then transferred to 6 well plates containing 10% FBS on the bottom. U251 siRNA transfected or LN229 shRNA transfected cells were plated (5×10^5cells/well) in triplicate wells of the upper chamber in serum free media. After 24 hours, cells were stained with 0.01% crystal violet, and the number of invading cells was counted at 20X magnification in 10 fields for each well.

Statistical tests

Unless otherwise specified experiments were done using 3 biological replicates and data is shown as average +/- sd., and statistical analysis was done using a 2-tailed student *t*-test.

S.C. xenograft tumor model

Hsd:Athymic Nude-Foxn1nu nude mice at age 5-6 weeks were used. For each cell line (LN229 or U251), 20 male nude mice were randomly assigned into two groups (n=10). Stably transfected LN229 and U251 cells were resuspended in pure culture medium with the concentration of 3×10^7 cells/ml. 100 ul cell suspension (3×10^6 cells) were inoculated subcutaneously (s.c.) into the lower right flank of the mice using 27 gauge needle. Tumor diameters are measured with digital calipers, and the tumor volume in mm^3 is calculated by the formula: Volume = $(width)^2\times length / 2$. The tumor size data were collected and processed blindly. The animal experiments were performed under the IRB approved animal protocol AWC-13-115.

Extended Data Legends

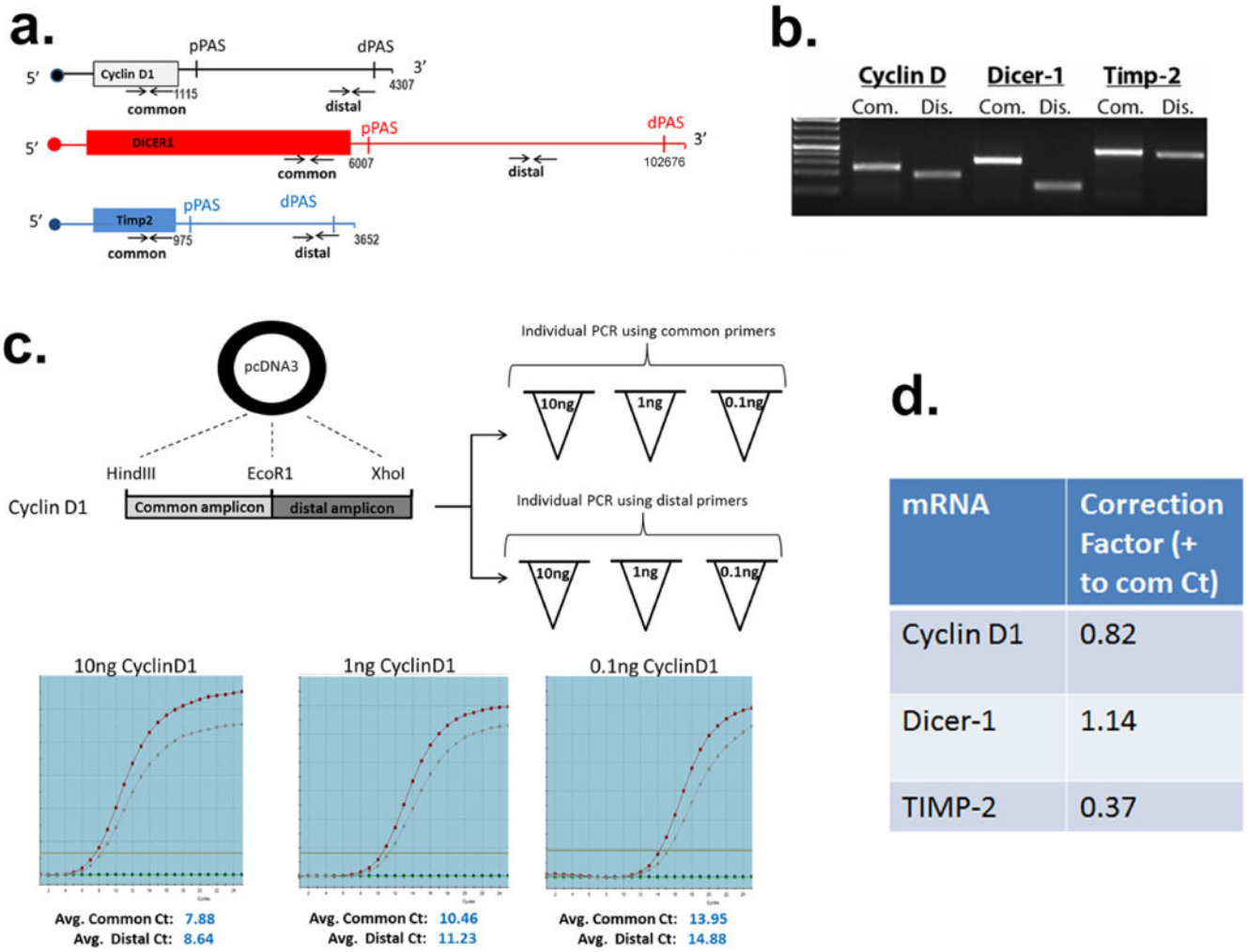

d.

mRNA	Correction Factor (+ to com Ct)
Cyclin D1	0.82
Dicer-1	1.14
TIMP-2	0.37

Extended Data Figure 1. Design and optimization of the qRT-PCR assay to monitor APA of three test genes

(a) Schematic denotes the relative location of the common and distal primer annealing sites in each test gene and the approximate locations of the annotated proximal and distal poly(A) sites depicted as pPAS and dPAS, respectively. The numbers demarcate where the 3′UTR starts and ends according to ENSEMBL. (b) Ethidium stained agarose gel of RT-PCR products of equal cycle number from the different amplicons using HeLa cell mRNA. (c) Both the common and distal Cyclin D1 amplicons were cloned into the same pcDNA3 plasmid in tandem. Three dilutions of each plasmid were made and amplified individually with each amplicon in triplicate. The 2 lines on the graph depict the amplification curve for the common and distal amplicons. The expectation is that identical Ct values should be attained for each, given that the PCR reactions were conducted using identical amounts of starting material. The average of 3 individual experiments is shown for each dilution and the average Ct deviation of either amplicon at all of the dilutions was calculated as a correction factor. (d) The experiment shown in panel c was repeated for Dicer-1 and Timp-2 to determine their respective correction factors, which was then applied to experiments shown in Figure 1.

a.

Samples	Control_r1	Control_r2	CFIm25kD_r1	CFIm25KD_r2
Mapped reads	269,463,902	270,426,980	265,270,708	282,404,060
#CDS	52.4%	47.6%	53.0%	51.5%
#5' UTR	5.2%	5.2%	5.5%	5.4%
#3' UTR	27.0%	23.4%	21.4%	20.3%
#Intron	6.3%	5.8%	6.0%	5.6%
#Intergenic	9.1%	17.9%	14.1%	17.3%
3' UTR average coverage	236	205	184	185

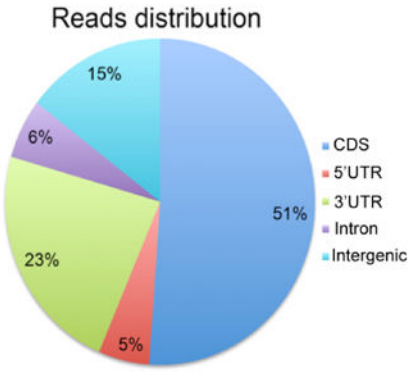

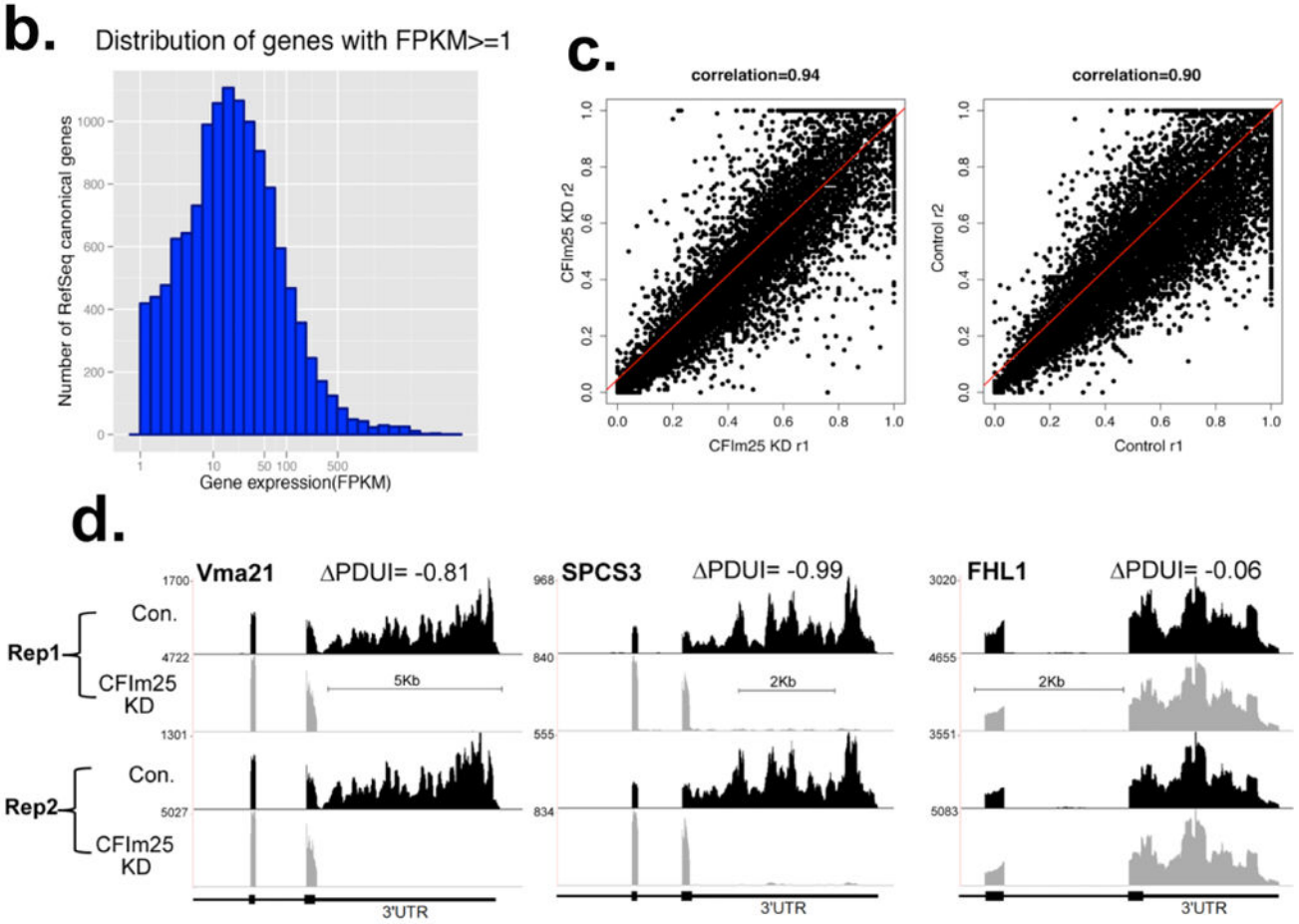

Extended Data Figure 2. Summary of RNA-Seq alignment and reproducibility of PDUI and CFIm25 depletion-induced 3′UTR shortening

(a) RNA-seq read statistics of the four biologically independent experiments where HeLa cells with treated with either control siRNA (Control) or CFIm25 siRNA (CFIm25kD). Pie chart on the right represents genomic distribution of reads that were mapped to human genome hg19. The percentage was calculated by averaging all samples. CDS: coding region. (b) Histogram of gene expression of RefSeq genes with FPKM (Fragments per Kilobase of transcript sequence per million mapped paired-end reads) no less than 1. (c) Scatterplot of the two biological replicates for each condition with high Pearson correlation ($r \geq 0.9$)

demonstrating a high level of reproducibility between sample PDUI scores. Each dot represents the PDUI of a transcript. (d) Genome browser screen images from four independent RNA-seq experiments. Each represents an independent biological sample where HeLa cells were transfected with either the control siRNA (Con.) or an siRNA that knocked down CFIm25. Both Vma21 and SPCS3 were found to undergo 3′UTR shortening after CFIm25 knockdown while FHL1 was found not to change.

a.

Samples	Control_r1	Control_r2	CFIm25kD_r1	CFIm25KD_r2
Mapped reads	269,463,902	270,426,980	265,270,708	282,404,060
#CDS	52.4%	47.6%	53.0%	51.5%
#5' UTR	5.2%	5.2%	5.5%	5.4%
#3' UTR	27.0%	23.4%	21.4%	20.3%
#Intron	6.3%	5.8%	6.0%	5.6%
#Intergenic	9.1%	17.9%	14.1%	17.3%
3' UTR average coverage	236	205	184	185

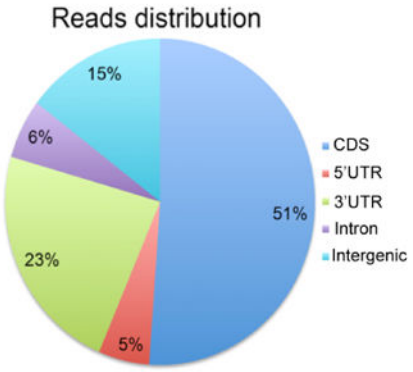

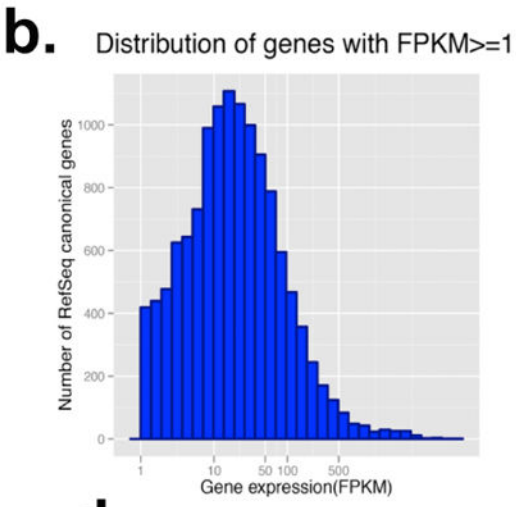

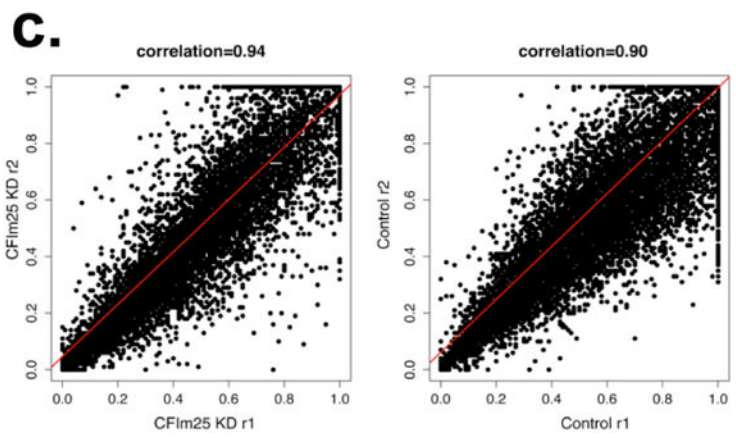

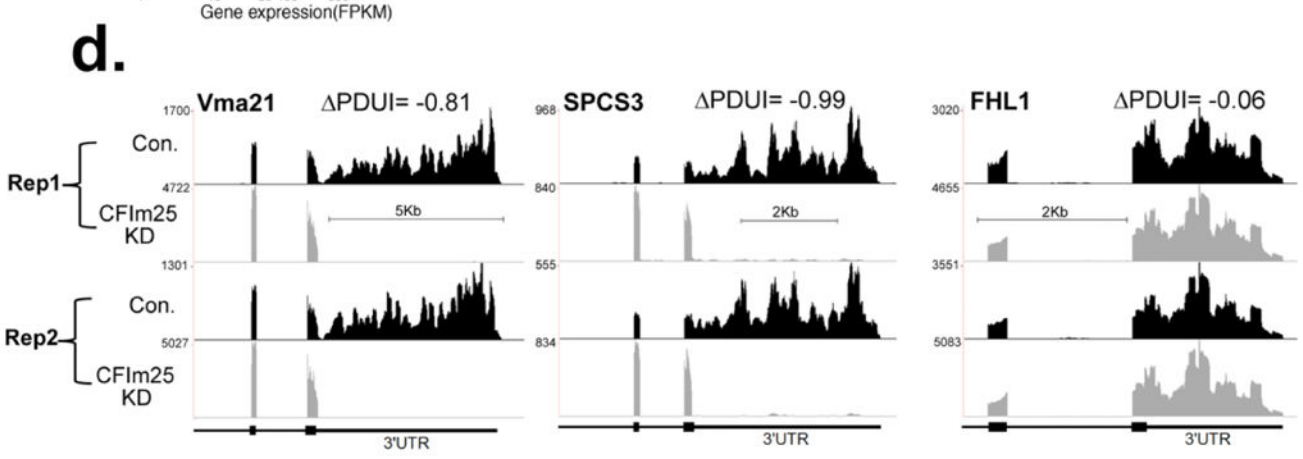

Extended Data Figure 3. Shortened transcripts have more "UGUA" CFIm25 binding motifs than unaltered transcripts

(a) CFIm25 is known to bind to the UGUA motif. The number of UGUA motifs within the 3′UTRs of genes with 3′UTR shortening after CFIm25 knockdown relative to genes with unaltered 3′UTRs was calculated and compared. Here we selected the genes without 3′UTR change according to |ΔPDUI|≤0.05. (b) iCLIP tags from Martin *et al* (GEO accession number GSE37398) was superimposed onto data derived from PDUI analysis of CFIm25 knockdown cells. The box plot demonstrates the enrichment of CFIm25 binding within 3′UTRs that are altered after CFIm25 knockdown (P = 6.1e-107, t-test).

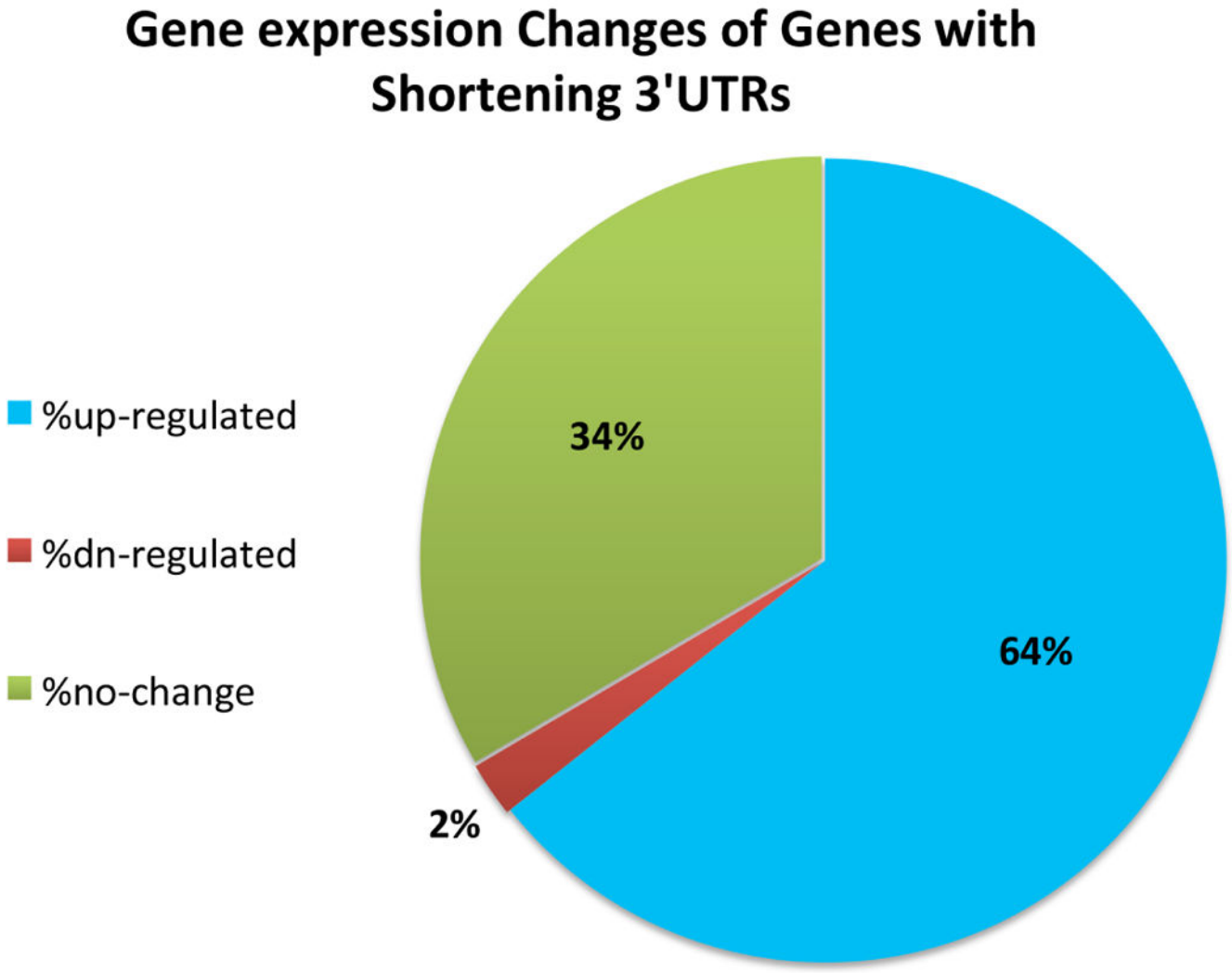

Extended Data Figure 4. Gene expression changes of genes with shortened 3′UTRs

Pie graph was calculated from the list of 1,450 genes exhibiting shortened 3′UTRs due to CFIm25 knockdown. The differentially expressed gene analysis was performed using edgeR with FDR ≤ 0.05 (see Methods)

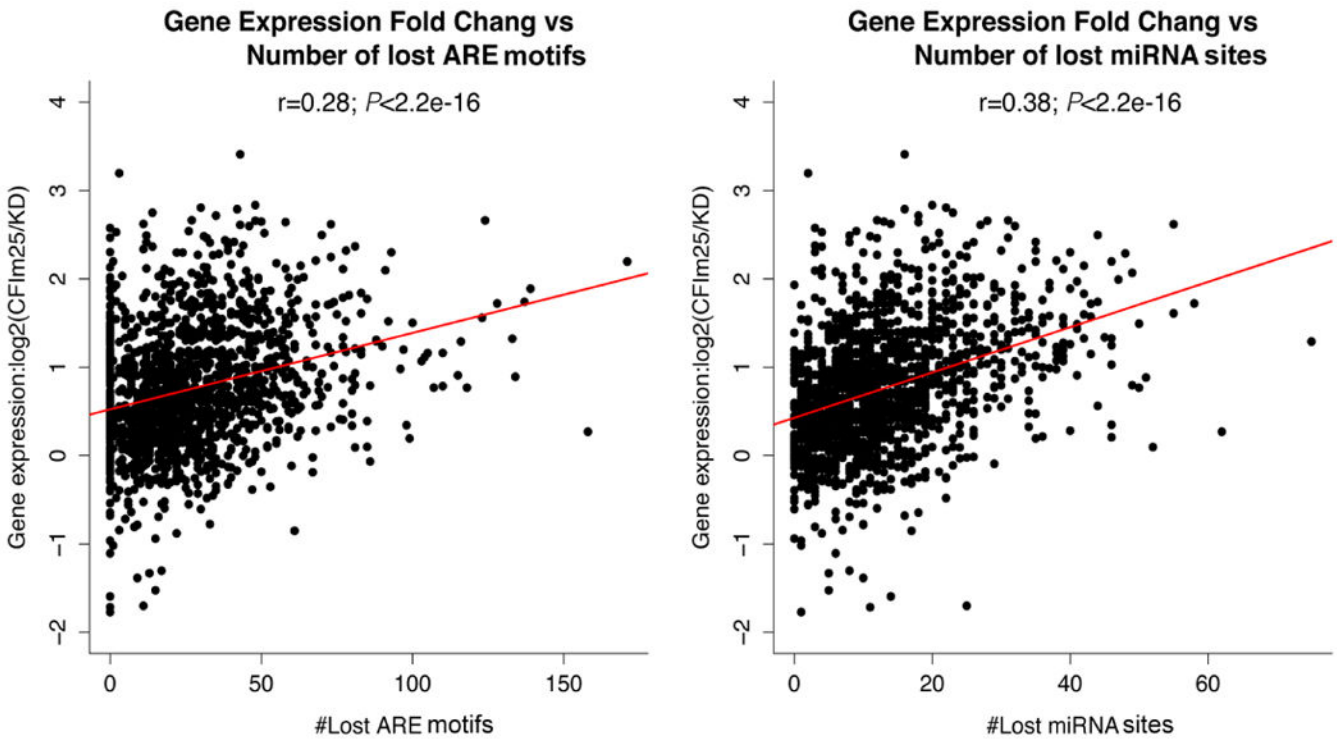

Extended Data Figure 5. The Pearson correlation between gene expression fold change and the number of lost negative regulatory elements

Left panel, the number of lost AREs due to 3′UTR shortening was calculated using the ARE database and plotted against change in gene expression levels after CFIm25 knockdown. Right panel, similar to the left except the number of lost patented miRNA target sites (Targetscan 6.2) was plotted.

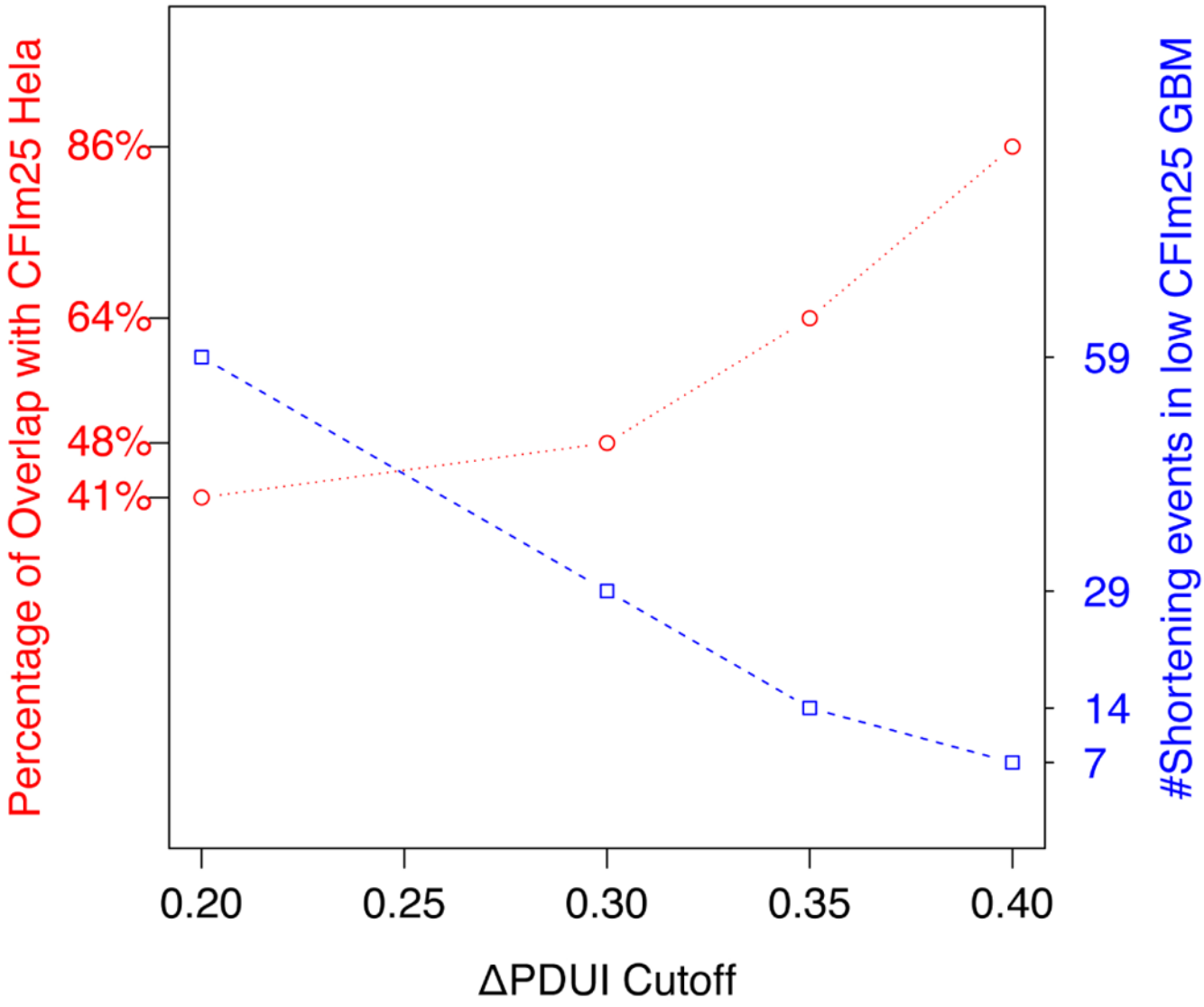

Extended Data Figure 6. Overlap between shortening events in GBM with low CFIm25 and shortening events in HeLa cells after CFIm25 Knockdown

Left Y-axis (red) represents the percentage of shortening events in low CFIm25 GBM which are also shortened in HeLa cells following CFIm25 knockdown. Right Y-axis (blue) represents the number of shortening events in low CFIm25 GBM against different |ΔPDUI| cutoffs.

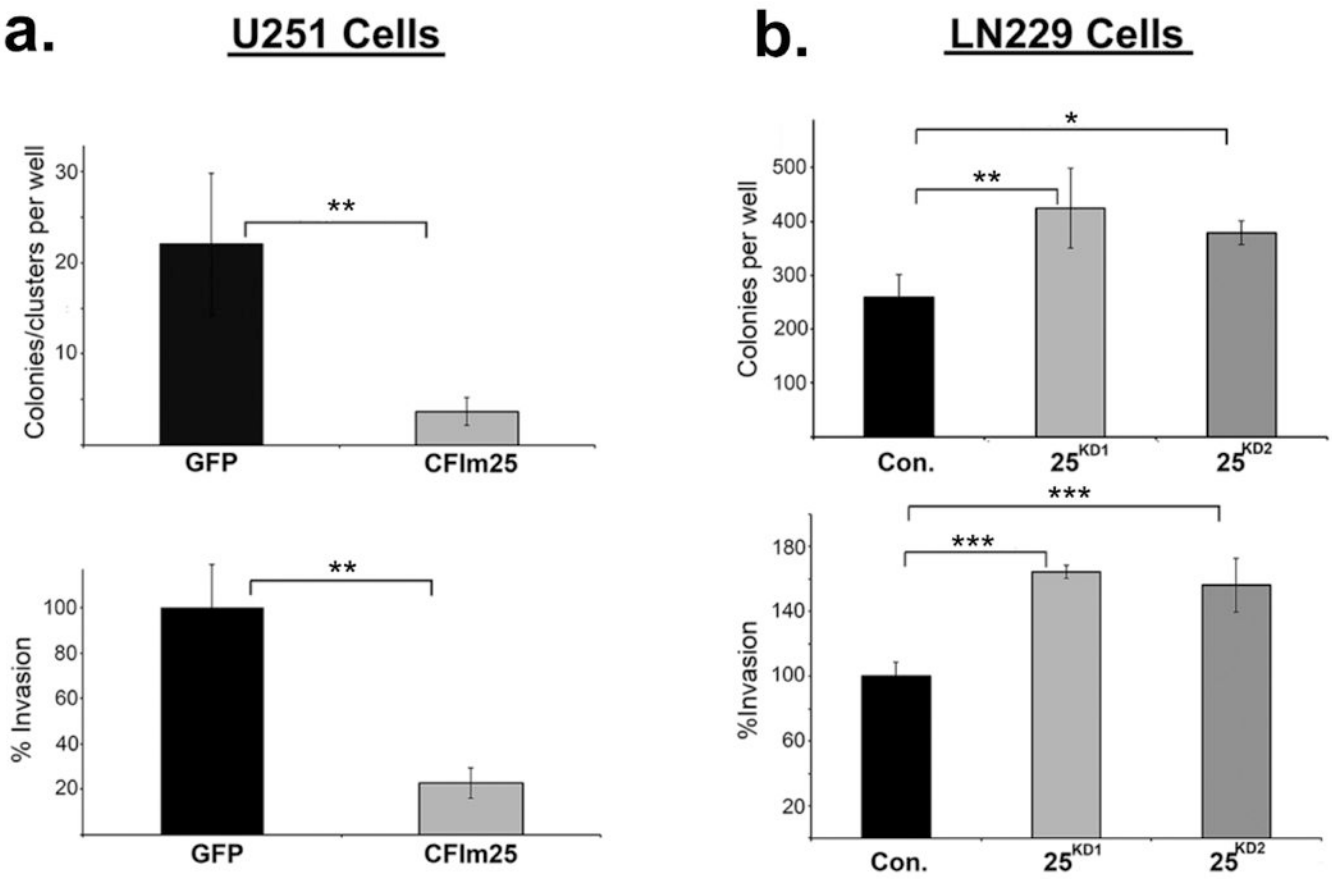

Extended Data Figure 7. Overexpression of CFIm25 reduces invasion and colony formation while CFIm25 depletion increases invasion and colony formation

(a) U251 cells were transfected with either GFP or CFIm25. Top left panel, Cells were replated in soft agar and the number of colonies/clusters formed were determined. Lower left panel, Matrigel invasion assay for cells overexpressing CFIm25 or GFP. (b) Top right panel, LN229 cells were transfected with either control or two different lentiviral plasmids targeting CFIm25 (KD1 and KD2). Stably transfected cells were plated on soft agar and the resulting colonies were counted for KD1 and KD2 respectively. Lower right panel, LN229 cells were transfected with either control or two different siRNAs (KD1 and KD2) directed against CFIm25 and were replated for a matrigel invasion assay. All the experiments were done in triplicate and shown is the mean ± standard deviation. All p-values were from the 2-tailed student *t*-test of the control vs. sample. **P*<0.1, ***P*<0.01, ****P*<0.001.

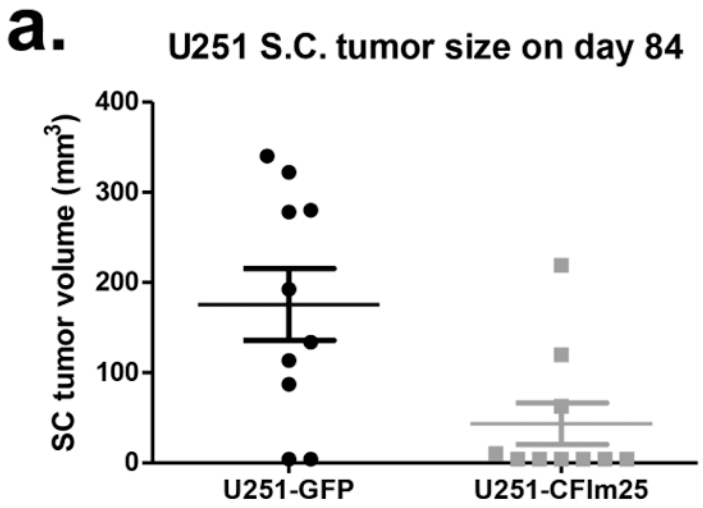

Table Analyzed	U251 S.C. tumor size on day 84
Column A	U251-GFP
vs	vs
Column B	U251-CFIm25
Unpaired t test	
P value	0.0102
P value summary	*
Are means signif. different? (P < 0.05)	Yes
One- or two-tailed P value?	Two-tailed
t, df	t=2.869 df=18

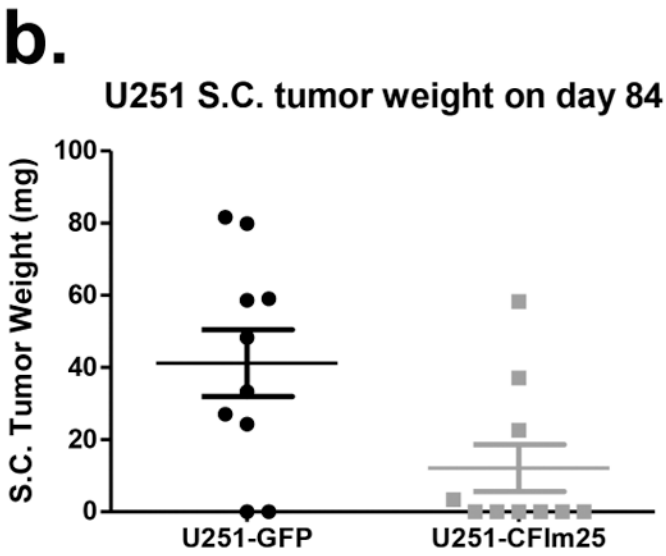

Table Analyzed	U251 S.C. tumor weight on day 84
Column A	U251-GFP
vs	vs
Column B	U251-CFIm25
Unpaired t test	
P value	0.0197
P value summary	*
Are means signif. different? (P < 0.05)	Yes
One- or two-tailed P value?	Two-tailed
t, df	t=2.560 df=18

Extended Data Figure 8. Overexpression of CFIm25 in U251 tumors reduces their size and weight

U251 xenograft tumors were isolated from nude mice on day 84 post implantation and measured for volume (a) and weight (b) (n=10). U251-GFP represents control U251 cells expressing GFP while U251-CFIm25 represents cells transduced with a lentivirus that over-expresses CFIm25.

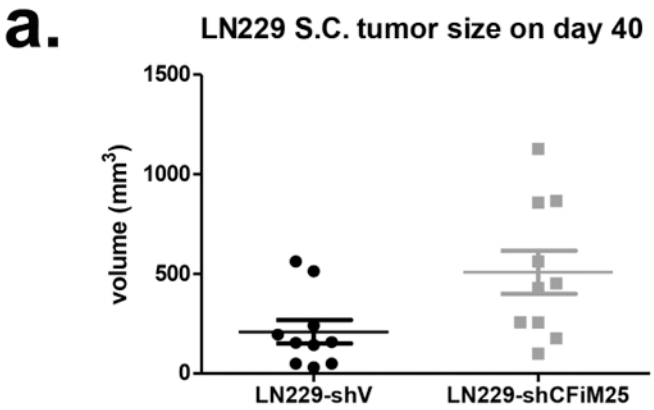

Unpaired t test	
P value	0.0257
P value summary	*
Are means signif. different? (P < 0.05)	Yes
One- or two-tailed P value?	Two-tailed
t, df	t=2.431 df=18

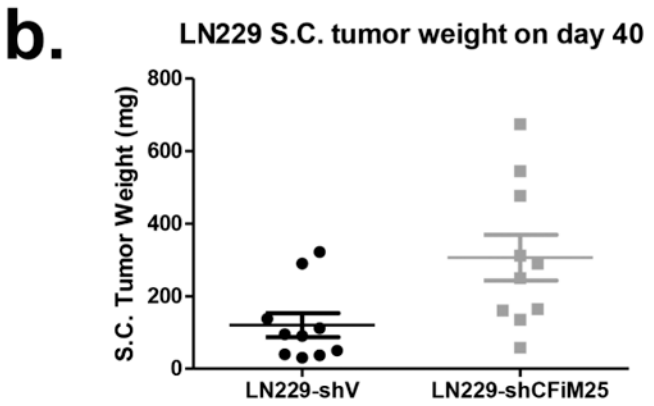

Unpaired t test	
P value	0.0173
P value summary	*
Are means signif. different? (P < 0.05)	Yes
One- or two-tailed P value?	Two-tailed
t, df	t=2.621 df=18

Extended Data Figure 9. Reduction in CFIm25 expression levels enhances LN229 tumor size and weight

LN229 xenograft tumors were isolated from nude mice on day 40 post implantation and measured for volume (a) and weight (b) (n=10). LN-229-shCon. represents control lentiviral transduced cells while LN229-shCFIm25 represents cells transduced with a lentivirus that expresses shRNA targeting CFIm25.

Supplementary Material

Refer to Web version on PubMed Central for supplementary material.

Acknowledgments

We would like to thank members of the Wagner, Shyu, and Li laboratories for helpful discussions, Dr. Phillip Carpenter for reviewing the manuscript, and Drs. Qi Zhu and Tsaiwei Shan of LC Sciences for their efforts on the RNA-seq. This work was supported by a CPRIT grant to E.J.W. and A.-B. S. (RP100107), and in part by a Department of Defense grant to E.J. W. (W81XWH-11-1-0304), National Institutes of Health grants to A.-B. S. (GM046454), E.J.W. (CA167752 and CA166274) and an endowment from the Houston Endowment, Inc. (to A.-B. S.). Work in the Li, W laboratory is funded by grants from the Department of Defense (W81XWH-10-1-0501), CPRIT (RP110471-C3) and NIH (R01HG007538). Work in the Li, M laboratory is funded by grants from Dr. Marnie Rose Foundation, and the William and Ella Owens Medical Research Foundation. CPM acknowledges a Department of Defense Postdoctoral Innovator Award (W81XWH-12-1-0218).

References

1. Elkon R, et al. E2F mediates enhanced alternative polyadenylation in proliferation. Genome Biol. 2012; 13:R59. [PubMed: 22747694]
2. Sandberg R, Neilson JR, Sarma A, Sharp PA, Burge CB. Proliferating cells express mRNAs with shortened 3′ untranslated regions and fewer microRNA target sites. Science. 2008; 320:1643–1647. [PubMed: 18566288]
3. Mayr C, Bartel DP. Widespread shortening of 3′UTRs by alternative cleavage and polyadenylation activates oncogenes in cancer cells. Cell. 2009; 138:673–684. [PubMed: 19703394]
4. Ji Z, Lee JY, Pan Z, Jiang B, Tian B. Progressive lengthening of 3′ untranslated regions of mRNAs by alternative polyadenylation during mouse embryonic development. Proceedings of the National Academy of Sciences. 2009; 106:7028–7033.
5. Mangone M, et al. The landscape of C. elegans 3′UTRs. Science. 2010; 329:432–435. [PubMed: 20522740]
6. Tian B, Hu J, Zhang H, Lutz CS. A large-scale analysis of mRNA polyadenylation of human and mouse genes. Nucleic Acids Research. 2005; 33:201–212. [PubMed: 15647503]
7. Di Giammartino DC, Nishida K, Manley JL. Mechanisms and consequences of alternative polyadenylation. Mol Cell. 2011; 43:853–866. [PubMed: 21925375]
8. Chen CYA, Shyu AB. AU-rich elements: characterization and importance in mRNA degradation. Trends in Biochemical Sciences. 1995; 20:465–470. [PubMed: 8578590]
9. Farh KK, et al. The widespread impact of mammalian MicroRNAs on mRNA repression and evolution. Science. 2005; 310:1817–1821. [PubMed: 16308420]
10. Wu L, Belasco JG. Let me count the ways: mechanisms of gene regulation by miRNAs and siRNAs. Mol Cell. 2008; 29:1–7. [PubMed: 18206964]
11. Singh P, et al. Global Changes in Processing of mRNA 3′ Untranslated Regions Characterize Clinically Distinct Cancer Subtypes. Cancer Res. 2009; 69:9422–9430. [PubMed: 19934316]
12. Kubo T, Wada T, Yamaguchi Y, Shimizu A, Handa H. Knock-down of 25 kDa subunit of cleavage factor Im in Hela cells alters alternative polyadenylation within 3′-UTRs. Nucleic Acids Res. 2006; 34:6264–6271. [PubMed: 17098938]
13. Yao C, et al. Transcriptome-wide analyses of CstF64-RNA interactions in global regulation of mRNA alternative polyadenylation. Proc Natl Acad Sci U S A. 2012; 109:18773–18778. [PubMed: 23112178]
14. Martin G, Gruber, Andreas R, Keller W, Zavolan M. Genome-wide Analysis of Pre-mRNA 3′ End Processing Reveals a Decisive Role of Human Cleavage Factor I in the Regulation of 3′UTR Length. Cell Reports. 2012; 1:753–763. [PubMed: 22813749]
15. Thomas PE, et al. Genome-wide control of polyadenylation site choice by CPSF30 in Arabidopsis. Plant Cell. 2012; 24:4376–4388. [PubMed: 23136375]
16. Jan CH, Friedman RC, Ruby JG, Bartel DP. Formation, regulation and evolution of Caenorhabditis elegans 3′UTRs. Nature. 2011; 469:97–101. [PubMed: 21085120]

17. Shepard PJ, et al. Complex and dynamic landscape of RNA polyadenylation revealed by PAS-Seq. RNA. 2011; 17:761–772. [PubMed: 21343387]
18. Bernard D, et al. The methyl-CpG-binding protein MECP2 is required for prostate cancer cell growth. Oncogene. 2006; 25:1358–1366. [PubMed: 16331274]
19. Sicinski P, et al. Cyclin D1 provides a link between development and oncogenesis in the retina and breast. Cell. 1995; 82:621–630. [PubMed: 7664341]
20. Weinstat-Saslow D, et al. Overexpression of cyclin D1 mRNA distinguishes invasive and in situ breast carcinomas from non-malignant lesions. Nat Med. 1995; 1:1257–1260. [PubMed: 7489405]
21. Liu W, et al. Reprogramming of proline and glutamine metabolism contributes to the proliferative and metabolic responses regulated by oncogenic transcription factor c-MYC. Proc Natl Acad Sci U S A. 2012
22. Wang JB, et al. Targeting mitochondrial glutaminase activity inhibits oncogenic transformation. Cancer Cell. 2010; 18:207–219. [PubMed: 20832749]
23. Klein ME, et al. Homeostatic regulation of MeCP2 expression by a CREB-induced microRNA. Nat Neurosci. 2007; 10:1513–1514. [PubMed: 17994015]
24. Deshpande A, et al. 3′UTR mediated regulation of the cyclin D1 proto-oncogene. Cell Cycle. 2009; 8:3584–3592. [PubMed: 19838062]
25. Gao P, et al. c-Myc suppression of miR-23a/b enhances mitochondrial glutaminase expression and glutamine metabolism. Nature. 2009; 458:762–765. [PubMed: 19219026]
26. Miura P, Shenker S, Andreu-Agullo C, Westholm JO, Lai EC. Widespread and extensive lengthening of 3′ UTRs in the mammalian brain. Genome Res. 2013; 23:812–825. [PubMed: 23520388]
27. Ulitsky I, et al. Extensive alternative polyadenylation during zebrafish development. Genome Res. 2012; 22:2054–2066. [PubMed: 22722342]
28. Nakayama T, et al. Aberrant expression of Fra-2 promotes CCR4 expression and cell proliferation in adult T-cell leukemia. Oncogene. 2008; 27:3221–3232. [PubMed: 18071306]
29. Wagner EJ, Garcia-Blanco MA. RNAi-mediated PTB depletion leads to enhanced exon definition. Mol Cell. 2002; 10:943–949. [PubMed: 12419237]
30. Trapnell C, Pachter L, Salzberg SL. TopHat: discovering splice junctions with RNA-Seq. Bioinformatics. 2009; 25:1105–1111. [PubMed: 19289445]
31. Ward A, Dutton JR. Regulation of the Wilms' tumour suppressor (WT1) gene by an antisense RNA: a link with genomic imprinting? J Pathol. 1998; 185:342–344. [PubMed: 9828831]
32. Trapnell C, et al. Transcript assembly and quantification by RNA-Seq reveals unannotated transcripts and isoform switching during cell differentiation. Nat Biotechnol. 2010; 28:511–515. [PubMed: 20436464]
33. Kaplan PJ, Mohan S, Cohen P, Foster BA, Greenberg NM. The insulin-like growth factor axis and prostate cancer: lessons from the transgenic adenocarcinoma of mouse prostate (TRAMP) model. Cancer Res. 1999; 59:2203–2209. [PubMed: 10232609]
34. Fabian MR, Sonenberg N, Filipowicz W. Regulation of mRNA translation and stability by microRNAs. Annu Rev Biochem. 2010; 79:351–379. [PubMed: 20533884]
35. Braulke T, Dittmer F, Gotz W, von Figura K. Alteration in pancreatic immunoreactivity of insulin-like growth factor (IGF)-binding protein (IGFBP)-6 and in intracellular degradation of IGFBP-3 in fibroblasts of IGF-II receptor/IGF-II-deficient mice. Horm Metab Res. 1999; 31:235–241. [PubMed: 10226807]
36. Hu JF, et al. Lack of reciprocal genomic imprinting of sense and antisense RNA of mouse insulin-like growth factor II receptor in the central nervous system. Biochem Biophys Res Commun. 1999; 257:604–608. [PubMed: 10198258]
37. Ellis MJ, et al. Insulin-like growth factors in human breast cancer. Breast Cancer Res Treat. 1998; 52:175–184. [PubMed: 10066081]
38. Friedman RC, Farh KKH, Burge CB, Bartel DP. Most mammalian mRNAs are conserved targets of microRNAs. Genome Res. 2009; 19:92–105. [PubMed: 18955434]

39. Gomez-Angelats M, Teeguarden JG, Dragan YP, Pitot HC. Mutational analysis of three tumor suppressor genes in two models of rat hepatocarcinogenesis. Mol Carcinog. 1999; 25:157–163. [PubMed: 10411141]

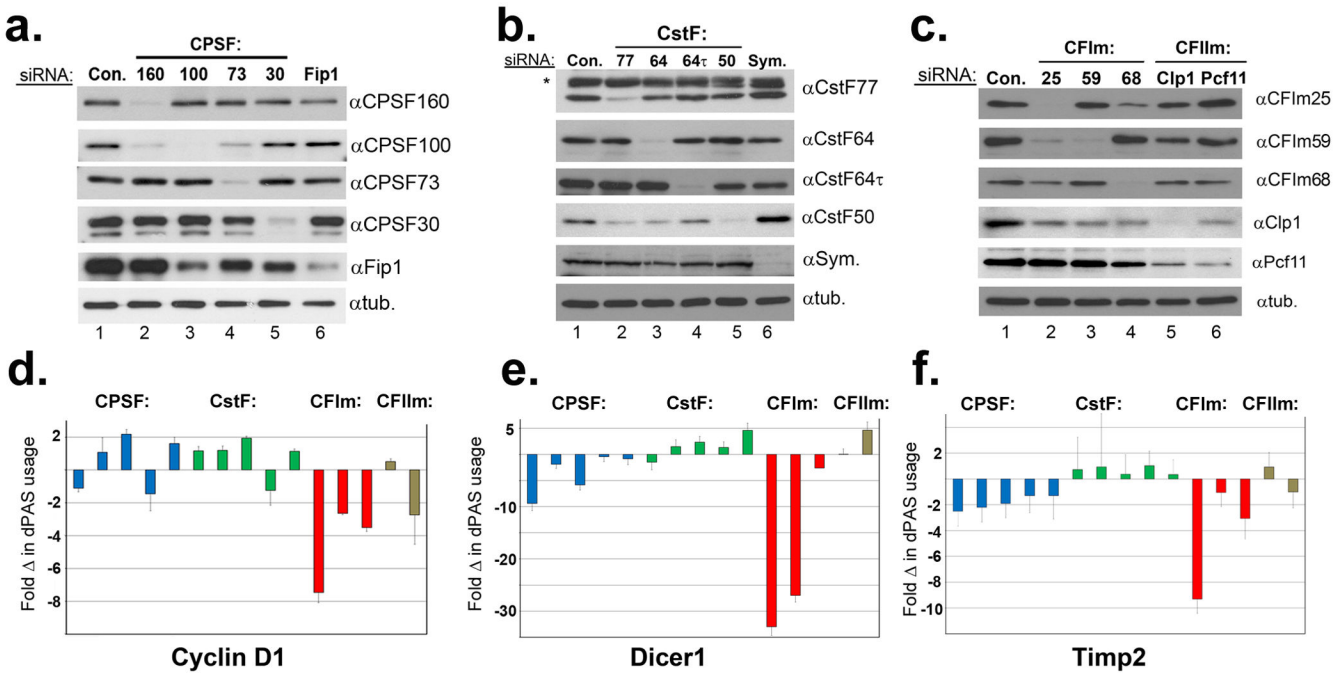

Figure 1. CFIm25 depletion leads to consistent and robust 3′UTR shortening of test genes

(a-c) Western blot analysis of HeLa cell lysates treated with control siRNA (Con.) and siRNAs individually targeting each of members of the CPA machinery. In all cases, tubulin was used as a loading control. (d-f) Quantified results of three biologically independent qRT-PCR experiments on RNA isolated from cells represented in panels A-C with the factors presented in the same order as shown in Westerns A-C. See methods for quantification details.

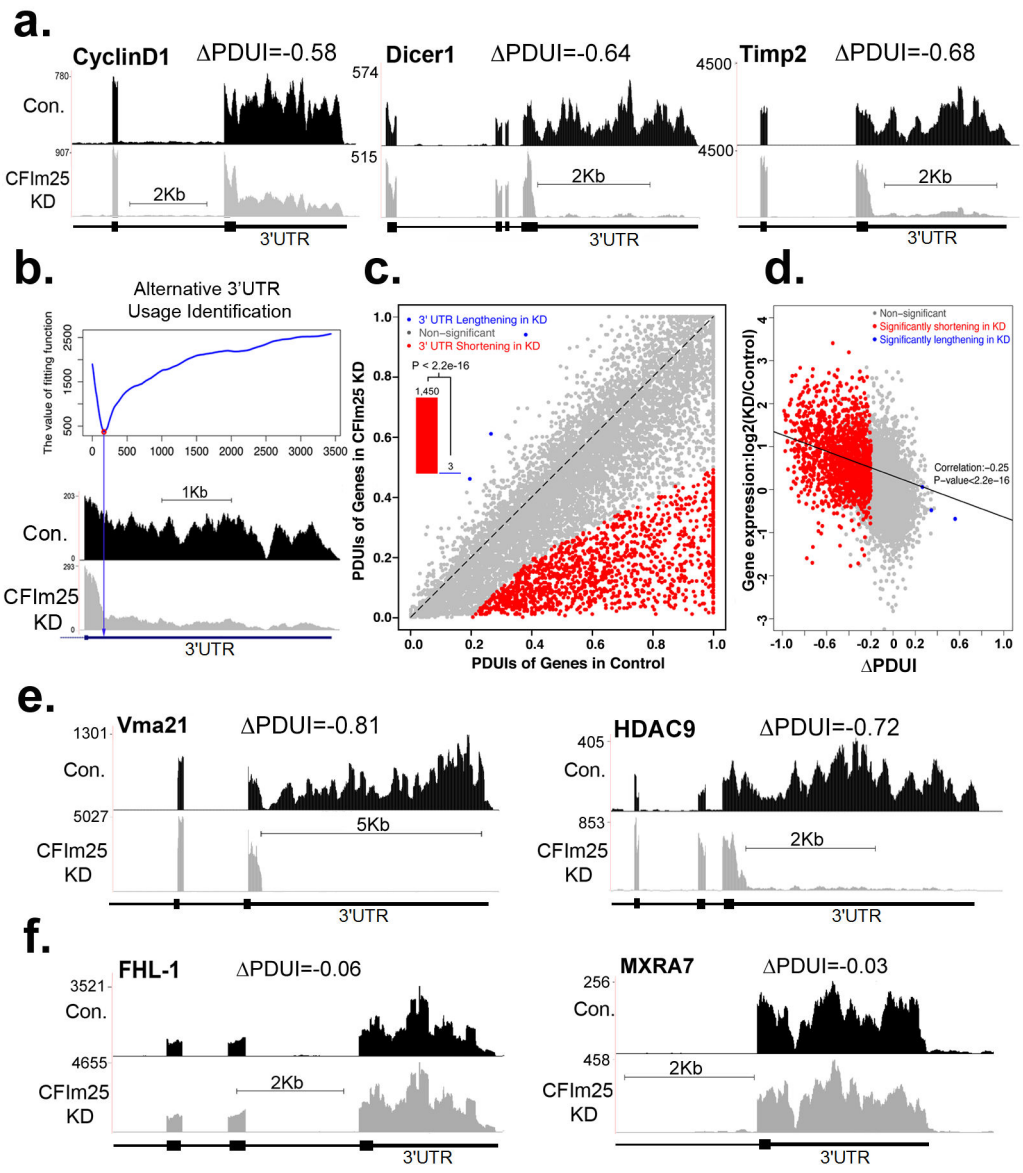

Figure 2. The DaPars algorithm identifies broad targets of CFIm25 in standard RNA-seq data

(a) RNA-seq read density for 3′UTR, terminal exon and upstream exon(s) after the control (Con.) siRNA treatment and CFIm25 knockdown (CFIm25KD) in HeLa cells. (b) Diagram depicts how the differential alternative 3′UTR usage was identified based on DaPars. Y-axis is the fitting value of the DaPars regression model and the locus with minimum fitting value (red point) is the predicted alternative pPAS for the RNA-seq data (below). (c) Scatterplot of PDUIs in control and CFIm25KD where mRNAs significantly shortened (n=1,450) or lengthened (n=3) after CFIm25KD (FDR ≤0.05, |ΔPDUI| ≥ 0.2 and at least two fold-change of PDUIs between CFIm25KD and control) are colored. The shifting towards proximal PAS is significant ($P < 2.2e{-}16$, binomial test). (d) Correlation between distal PAS site usage and gene expression levels of control and CFIm25KD. The x-axis denotes |ΔPDUI|; a negative value indicates that proximal PAS is prone to be used in CFIm25KD. The y-axis denotes the logarithm of the expression level of genes from the CFIm25KD relative to the control

sample. (e) Representative RNA-seq density plots along with ΔPDUI values for genes whose 3′UTR is shortened in response to CFIm25KD. (f) Representative RNA-seq density plots along with ΔPDUI values of genes whose 3′UTR is unchanged by CFIm25KD.

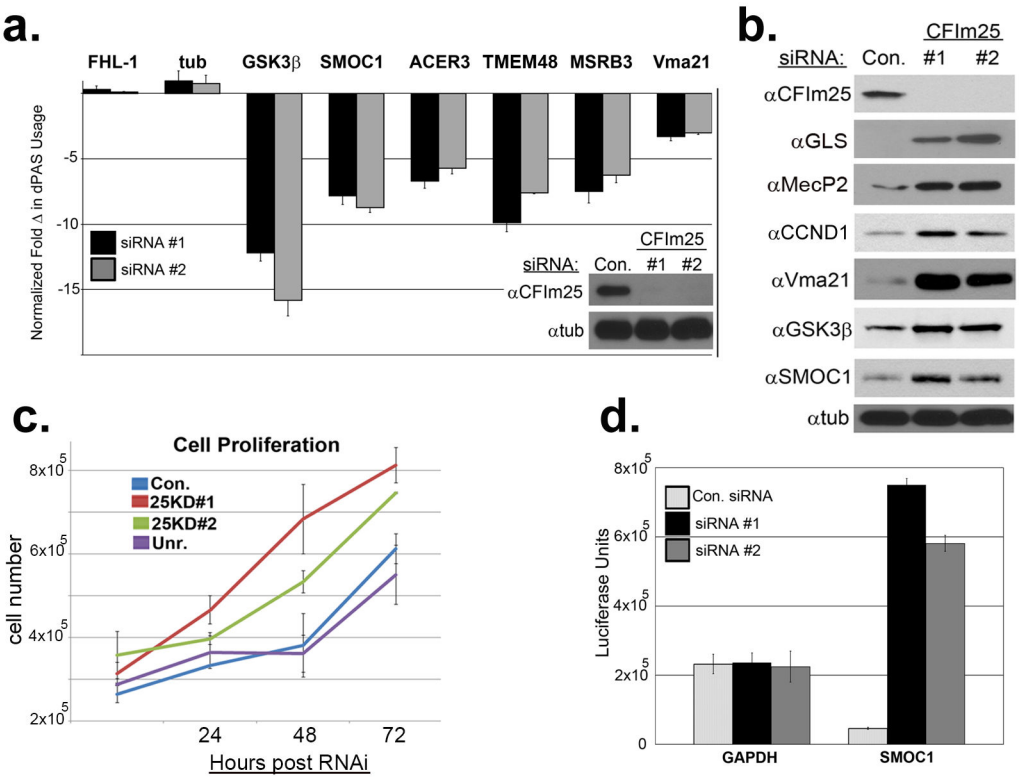

Figure 3. Increased pPAS usage after CFIm25 depletion results in increased protein translation and enhanced cell proliferation

(a) qRT-PCR results of select genes shown as fold change in dPAS usage after CFIm25 depletion. Experiments were performed in triplicate with standard error shown. The inset shows Western blot analysis demonstrating effective knockdown of CFIm25 using two distinct siRNAs. (b) Results of Western blot analysis of cell lysates after knockdown of CFIm25 using. (c) Growth of HeLa cells was measured after RNAi of CFIm25 compared to cells transfected with control or the siRNA to CFIImPcf11 (Unr.). Results shown are mean± s.d (*n*=3). (d) Graph representing luciferase activity from cells transfected with a luciferase reporter containing the 3′UTR of either GAPDH or of Smoc1 after being transfected with either control or CFIm25 siRNA. Data is the average of three independent experiments and error bars are their standard deviation.

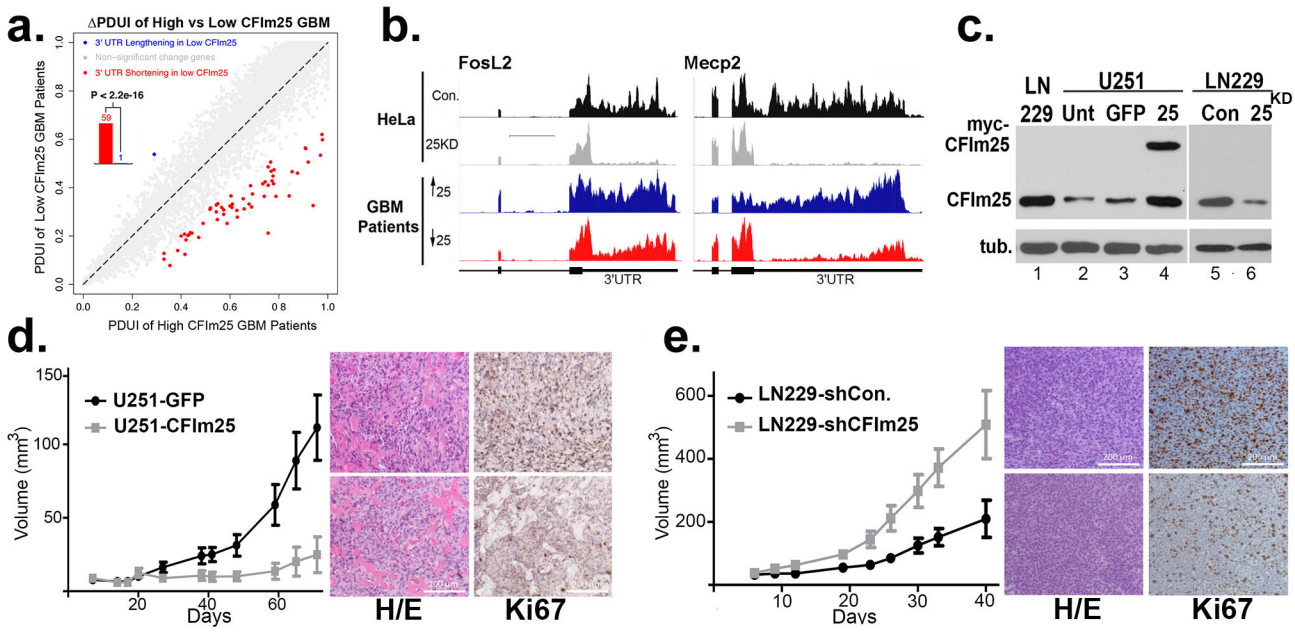

Figure 4. Altered expression of CFIm25 modulates GBM tumor growth

(a) The global analysis of 3′UTR changes in GBM patient samples with either high or low levels of CFIm25. Scatterplot of PDUIs from both datasets using the same cutoffs as in Figure 2c. The shifting to proximal PAS in the low CFIm25 group is significant (*P*<2.2e-16; binomial test). (b) Representative UCSC Genome Browser images of RNA-seq data demonstrating 3′UTR shortening after CFIm25 knockdown in HeLa and in GBM patient samples having high (blue) or low CFIm25 expression (red). (c) Western blot analysis of lysates from two GBM cell lines. Note the overexpressed myc-CFIm25 also increases endogenous CFIm25 levels in U251 cells. (d) Growth comparison of U251 tumors overexpressing either GFP (control) or CFIm25 and data represents the average of 10 mice per group. Right panel is representative H/E and Ki67 staining of U251-GFP tumors (upper) or U251-CFIm25 tumors (lower). (e) Growth comparison of LN229 tumors derived from cells transduced with lentiviruses expressing a scrambled shRNA (control) or with lentiviruses expressing shRNA targeting CFIm25. The data represents the average of 10 mice per group. Right panel is representative H/E and Ki67 staining of LN229 tumors expressing shRNA targeting CFIm25 (upper) or LN229 tumors expressing scrambled shRNA (lower).